ADVANCED FUNCTIONAL MATERIALS
www.afm-journal.de

Emergent Spin-Glass Behavior in an Iron(II)-Based Metal–Organic Framework Glass

Chinmoy Das, Soma Salamon, Joachim Landers, Jan-Benedikt Weiß, Wen-Long Xue, Pascal Kolodzeiski, Roman Pallach, Heiko Wende, and Sebastian Henke**

Metal–organic framework (MOF) glasses combine the structural tunability of crystalline MOFs with the processability of amorphous materials, offering exciting opportunities for functional hybrid materials. Here, a one-pot, solvent-free synthesis is reported of an Fe^{2+}-based MOF glass, *g*Fe-^{t}Bubipy, with the composition $[Fe_2(im)_{3.12}(bim)_{0.88}(^{t}Bubipy)_{0.11}]\cdot[Fe(Cp)_2]_{0.09}$ (im^- = imidazolate, bim^- = benzimidazolate, ^{t}Bubipy = 4,4′-di-*tert*-butyl-2,2′-bipyridine, Cp^- = cyclopentadienyl anion). This material forms a continuous random network structure of four-connected tetrahedral and octahedral Fe^{2+} nodes and exhibits an exceptionally low glass transition temperature (T_g = 87 °C). Despite its amorphous nature and complex composition, *g*Fe-^{t}Bubipy exhibits a high degree of local structural order that enables strong antiferromagnetic exchange interactions between Fe^{2+} centers. Remarkably, it exhibits clear signatures of spin-glass behavior, with a well-defined magnetic freezing transition ≈14 K. This combination of a MOF glass exhibiting a distinct glass transition with spin-glass magnetism arising from topological disorder and frustrated, short-range magnetic interactions represent a significant advance. This discovery underscores the transformative potential of MOF glasses as a versatile platform for exploring the interplay between structural disorder and cooperative magnetic phenomena in hybrid materials.

1. Introduction

Metal–organic framework (MOF) and coordination polymer (CP) glasses represent a new class of amorphous materials that combine the structural tunability of crystalline frameworks with the disorder and processability of glasses. Their unique properties, including porosity,[1–4] ionic conductivity,[5,6] gas separation capability,[7–9] mechanical robustness[10,11] and optical transparency,[12,13] have attracted significant attention for potential device integration. A key advantage of these glasses over their crystalline counterparts lies in the elimination of grain-boundary defects, which can improve mechanical integrity and facilitate shaping and processing.[7,8,13,14]

Among MOFs, zeolitic imidazolate frameworks (ZIFs) are the most prominent glass-formation systems. Their high thermal stability allows certain ZIFs to melt and vitrify upon cooling, yielding continuous random network (CRN) topologies reminiscent of inorganic oxide glasses.[15,16] However, the majority of reported ZIF glasses are based on Zn^{2+} centers and are thus diamagnetic. Paramagnetic ZIF glasses incorporating Fe^{2+},[17] Co^{2+},[18] and Cu^{2+}[19] centers have also been reported. Among these, only the magnetic properties of ZIF-62(Co), $Co(im)_{1.70}(bim)_{0.30}$ (im^- = imidazolate, bim^- = benzimidazolate) have been explored.[18] While crystalline ZIF-62(Co) exhibits antiferromagnetic ordering below a critical temperature (T_N = Néel temperature) of ≈12 K, its melt-quenched glass features impurities of metallic cobalt nanoparticles that mask the intrinsic magnetic properties of the Co-based glass network itself.[18]

In contrast to the ZIF glasses, several crystalline im^--based MOFs/CPs containing Fe^{2+} and Co^{2+} metal centers have demonstrated a rich variety of magnetic behaviors, including spin-crossover and antiferromagnetic ordering at low temperatures. These phenomena arise from exchange interactions mediated by imidazolate-type linkers, which connect the magnetic metal centers in the crystalline frameworks.[20–25] Most of these materials exhibit antiferromagnetic coupling between neighboring metal centers, although weak ferromagnetic-like behavior is often observed due to spin canting, which disrupts perfect antiparallel spin alignment.[18,20–22,25–28]

C. Das, J.-B. Weiß, W.-L. Xue, P. Kolodzeiski, R. Pallach, S. Henke
Anorganische Chemie
Fakultät für Chemie und Chemische Biologie
Technische Universität Dortmund
Otto-Hahn-Straße 6, 44227 Dortmund, Germany
E-mail: chinmoy.d@srmap.edu.in; sebastian.henke@tu-dortmund.de
C. Das
Department of Chemistry
SRM University-AP
Amaravati, Andhra Pradesh 522240, India
S. Salamon, J. Landers, H. Wende
Fakultät für Physik and Center for Nanointegration Duisburg-Essen (CENIDE)
Universität Duisburg-Essen
Lotharstraße 1, 47057 Duisburg, Germany

The ORCID identification number(s) for the author(s) of this article can be found under https://doi.org/10.1002/adfm.202517854

DOI: 10.1002/adfm.202517854

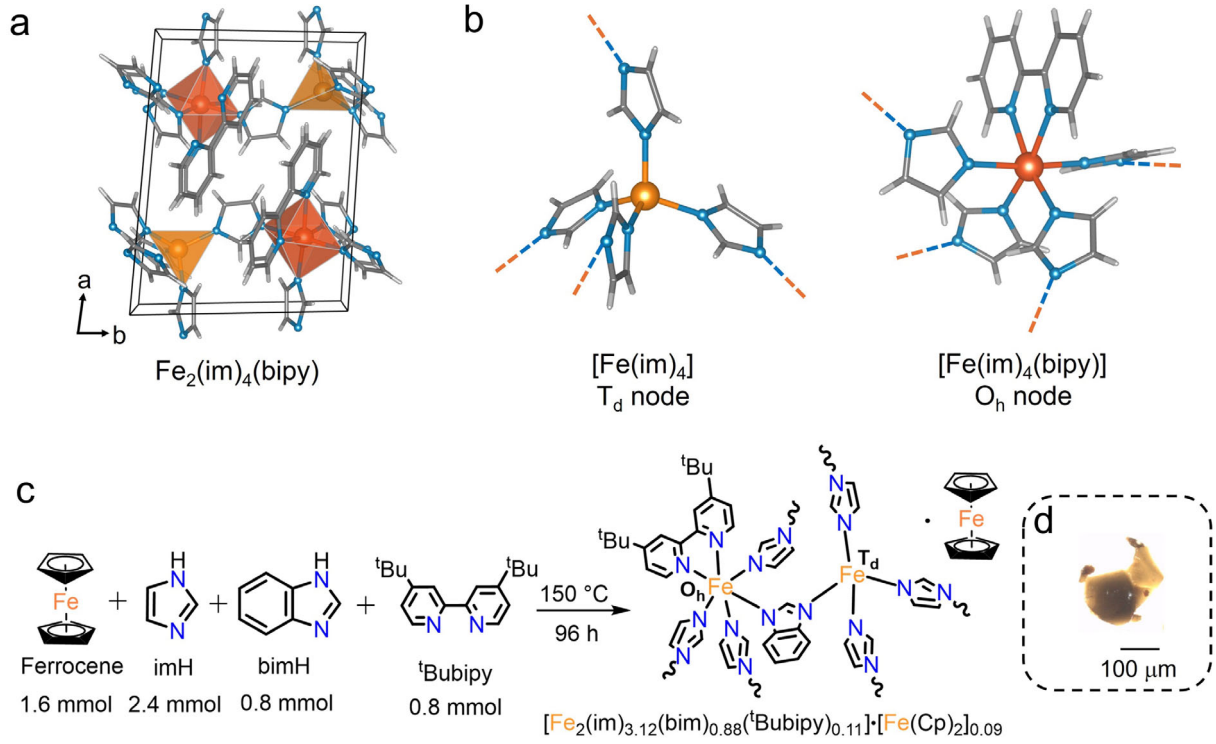

Figure 1. a) X-ray crystal structure of $Fe_2(im)_4(bipy)$ (CCDC code ICOTUQ) viewed along the *c*-axis.[25] b) Representation of four-fold connectivity of the tetrahedral [Fe(im)$_4$] units and four-fold seesaw-like connectivity in octahedral [Fe(im)$_4$(bipy)] units from the crystal structure of $Fe_2(im)_4(bipy)$. Fe^{2+} (O_h node), Fe^{2+} (T_d node), N, C, and H atoms are shown in dark orange, orange, blue, gray, and light gray. c) Schematic representation of one-pot synthesis of ***g*Fe-^{t}Bubipy**. d) Optical microscopy image of a ***g*Fe-^{t}Bubipy** glass shard, which was obtained by crushing the large glass monolith after purification.

The magnetic behavior of these systems can be further modulated by the introduction of additional capping ligands, such as, 2,2′-bipyridine (bipy) or 1,10-phenanthroline.[25,26] For instance, in $Fe_2(im)_4(bipy)$, which exhibits a crystalline layered framework structure, Fe^{2+} centers alternate between two coordination environments: tetrahedrally coordinated Fe^{2+} ions (local T_d symmetry) bound to four im^- linkers and octahedrally coordinated Fe^{2+} ions (local O_h symmetry) bound to four im^- linkers and a chelating bipy ligand (**Figure 1**a,b). $Fe_2(im)_4(bipy)$ displays a two-step partial spin-crossover accompanied by structural phase transitions between 155 and 130 K, resulting in a mix of high-spin and low-spin Fe^{2+} centers. Below the T_N of 4 K, the remaining high-spin Fe^{2+} centers undergo antiferromagnetic ordering with spin canting, further showcasing the tunable magnetic properties achievable in these frameworks.[25]

Despite this well-established behavior in crystalline frameworks, little is known about how such magnetic exchange interactions manifest in the amorphous, topologically disordered networks of MOF glasses. Specifically, the possibility of cooperative magnetic phenomena such as spin-glass freezing[29–37] in disordered MOF-derived glasses has remained unexplored. Spin glasses are characterized by the collective freezing of interacting spins into a disordered, metastable state due to frustration and randomness in exchange pathways. As such, spin glasses have a fundamentally different ground state from long-range ordered antiferromagnets or ferromagnets.[30,32,38]

Here, we report the solvent-free, one-pot synthesis of the Fe^{2+}-based MOF glass, $[Fe_2(im)_{3.12}(bim)_{0.88}(^tBubipy)_{0.11}]\cdot[Fe(Cp)_2]_{0.09}$ (hereafter referred to as ***g*Fe-^{t}Bubipy**), prepared by reacting ferrocene ($Fe(Cp)_2$, Cp^- = cyclopentadienyl anion) with a mixture of imH, bimH and 4,4′-di-*tert*-butyl-2,2′-bipyridine (^{t}Bubipy). The introduction of the bulkier ^{t}Bubipy ligand in place of bipy, along with the partial substitution of im^- by bim^- linkers, effectively disrupts crystallization, promoting direct glass formation through structural perturbation.[39,40] Structural analyses reveal that ***g*Fe-^{t}Bubipy** adopts a four-connected CRN structure comprising tetrahedral (T_d, [Fe(im/bim)$_4$]) and octahedral (O_h, [Fe(im/bim)$_4$(^{t}Bubipy)]) nodes. Importantly, the glassy material features short-range antiferromagnetic coupling among bridged Fe^{2+} centers within the disordered network and shows clear signatures of spin-glass behavior,[32,35,36,41,42] with a well-defined spin-freezing transition at $T_F = 14$ K (T_F = freezing temperature) and magnetic hysteresis consistent with a frozen, disordered spin configuration. This work demonstrates that MOF glasses with a CRN topology can host cooperative magnetic phenomena such as spin-glass freezing, offering a new platform for systematically exploring magnetic frustration and disorder in amorphous coordination materials.

2. Results and Discussion

2.1. Synthesis, Compositional and Structural Analysis

The solvent-free, one-pot solid-state synthesis[20,27,28] of ***g*Fe-^{t}Bubipy** was carried out by reacting $Fe(Cp)_2$, imH, bimH and ^{t}Bubipy in vacuum-sealed Carius tubes (Figure 1c; Figure S1,

Supporting Information). The mixture was heated isothermally at 150 °C for 4 days, followed by thorough washing under inert conditions. This approach builds on the established protocol for synthesizing crystalline $Fe_2(im)_4(bipy)$,[25] but the substitution of bipy with the bulkier ^{t}Bubipy and the partial replacement of im^- by bim^- linkers introduce structural perturbations that prevent the formation of a crystalline coordination network. As a result, ***g*Fe-^{t}Bubipy** forms an amorphous phase, evidenced by the absence of sharp Bragg peaks and the presence of broad diffuse scattering in powder X-ray diffraction (PXRD) patterns (**Figure 2a**). Similar strategies using bim^- substitution to introduce amorphization have been reported for other imidazolate-based MOF systems.[43]

Optical microscopy imaging shows ***g*Fe-^{t}Bubipy** as monolithic particles with a dark-brown appearance (Figure 1d). This intense color contrasts sharply with the typical orange hue of Fe^{2+}-based ZIFs,[17,44] but aligns with the dark-green color reported for crystalline $Fe_2(im)_4(bipy)$.[20] The pronounced color is attributed to metal-to-ligand charge-transfer (MLCT) transitions from Fe^{2+} to ^{t}Bubipy.[45–47]

Thermogravimetric analysis (TGA) under O_2 flow provided the iron mass fraction (Figure S2, Supporting Information), while the molar ratio of the organic ligands was quantified by solution ^{1}H NMR spectroscopy of an acid-digested sample (Figure S5, Supporting Information). These analyses confirm the composition $[Fe_2(im)_{3.12}(bim)_{0.88}(^t\text{Bubipy})_{0.11}]\cdot[Fe(Cp)_2]_{0.09}$ for ***g*Fe-^{t}Bubipy**, consistent with Fe in the +II oxidation state, as expected for Fe-based MOFs prepared by analogous solvent-free methods under inert conditions.[17,20,27,28] Notably, a small amount of residual $Fe(Cp)_2$ remains in the material despite extensive washing, which we attribute to its encapsulation with the glass network. Like typical crystalline iron imidazolate MOFs, ***g*Fe-^{t}Bubipy** is sensitive to hydrolysis and oxidation in air and was therefore stored and handled under inert conditions using glovebox and Schlenk techniques.

Based on the determined composition, with only ≈0.11 ^{t}Bubipy ligands per two Fe^{2+} centers, ≈6% of Fe^{2+} sites are expected to adopt an octahedral (O_h) $[FeN_6]$ environment due to coordination by ^{t}Bubipy and four im^-/bim^- linkers, while the remaining ≈94% feature tetrahedral (T_d) $[FeN_4]$ coordination with four im^-/bim^- linkers only. Beyond the characteristic dark color associated with the $[Fe(^t\text{Bubipy})(im/bim)_4]$ nodes, coordination of the ^{t}Bubipy ligand to Fe^{2+} centers was also confirmed by Fourier-transform infrared (FTIR) spectroscopy. The prominent ring breathing vibration of ^{t}Bubipy shifts from 605 to 619 cm^{-1} in ***g*Fe-^{t}Bubipy** (Figure 2b), consistent with transition metal coordination.[48–51] Similar to Zn^{2+}- and Co^{2+}-based ZIFs, vibrational bands between 250 and 300 cm^{-1} in the FTIR spectrum of ***g*Fe-^{t}Bubipy** are assigned to Fe—N stretching vibrations of $[FeN_4]$ tetrahedra.[3,19] This assignment is supported by density functional theory (DFT) calculations on the dianionic model complex $[Fe(im)_4]^{2-}$ representing the T_d nodes in ***g*Fe-^{t}Bubipy** (Figure 2c; Figure S11, Supporting Information calculated stretching frequencies are located between 262 and 295 cm^{-1}).

Additional DFT calculations were performed for the model complex $[Fe(^t\text{Bubipy})(im)_4]^{2-}$ to predict Fe—N stretching frequencies of the octahedral ^{t}Bubipy-coordinated $[FeN_6]$ nodes (Figure 2c). Given that octahedral Fe^{2+} complexes with intermediate-

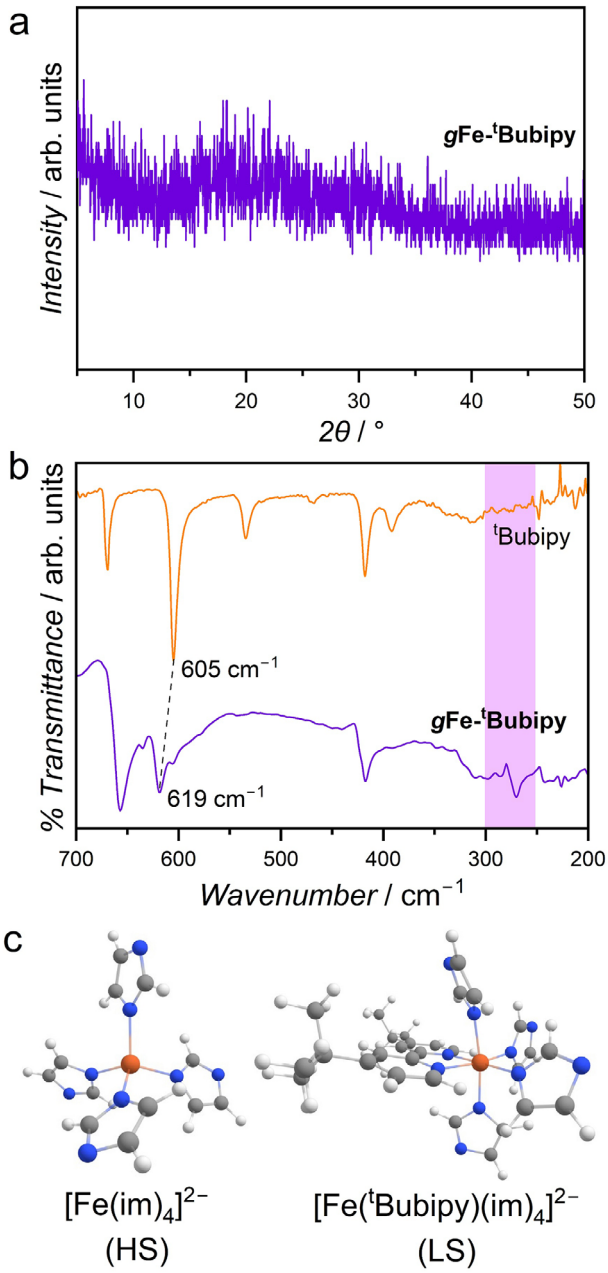

Figure 2. a) PXRD pattern of ***g*Fe-^{t}Bubipy**. b) FTIR spectrum of ***g*Fe-^{t}Bubipy** compared with that of the free ^{t}Bubipy ligand. The bands at 619 and 605 cm^{-1} are assigned to a ring breathing vibration of ^{t}Bubipy. The pink-highlighted region (250-300 cm^{-1}) indicates where Fe—N stretching vibrations of tetrahedral $[FeN_4]$ units are expected, based on DFT-calculated vibrational frequencies of the anionic model complex $[Fe(im)_4]^{2-}$. c) Visualization of selected DFT-optimized model structures for the tetrahedral node $[Fe(im)_4]^{2-}$ and the octahedral node $[Fe(^t\text{Bubipy})(im)_4]^{2-}$ (HS = high spin, LS = low spin).

to strong-field ligands, such as ^{t}Bubipy, can adopt both high-spin (S = 2) and low-spin (S = 0) configurations, both spin states were evaluated. Fe—N stretching frequencies were predicted between 225 and 265 cm^{-1} for the high-spin variant and 375–385 cm^{-1} for the low-spin variant (Figures S12 and S13,

Supporting Information). However, the experimental FTIR spectrum of ***g*Fe-^{t}Bubipy** is too noisy in these regions to unambiguously assign bands to these modes, likely due to the very small concentration of the octahedral [FeN_6] species in ***g*-Fe^{t}Bubipy** and its disordered structure leading to broad vibrational bands.

To gain deeper insights into the local structure of ***g*Fe-^{t}Bubipy**, X-ray total scattering data were collected and compared with experimental data for the crystalline reference compounds $Fe_2(im)_4(bipy)$ (Figure S6 and Table S1, Supporting Information) (CCDC: ICOTUQ)[25] and $Fe_3(im)_6(imH)_2$ (Figure S7 and Table S2, Supporting Information) (CCDC: IMIDFE).[20] $Fe_3(im)_6(imH)_2$, the precursor to the Fe^{2+}-based ZIF glass former $Fe(im)_2$, features a 2:1 ratio of T_d and O_h Fe^{2+} nodes, whereas $Fe_2(im)_4(bipy)$ displays a 1:1 ratio. Additionally, the O_h nodes in $Fe_3(im)_6(imH)_2$ are *trans*-coordinated by two terminal imH ligands, contrasting with the *cis*-coordination of bipy in $Fe_2(im)_4(bipy)$. Despite these differences, both reference materials share highly ordered networks built from tetrahedral and octahedral Fe^{2+} coordination motifs. The total scattering functions $S(Q)$ of the crystalline $Fe_2(im)_4(bipy)$ and $Fe_3(im)_6(imH)_2$ show sharp Bragg peaks characteristic of their ordered structures, whereas ***g*Fe-^{t}Bubipy** displays only broad, diffuse scattering, consistent with its amorphous network structure (**Figure 3a**). Pair distribution functions (PDFs) in the form $D(r)$ derived from $S(Q)$ via Fourier transformation, reveal that up to a correlation length (r) of ≈6.1 Å, the local structure of ***g*Fe-^{t}Bubipy** closely resembles those of the crystalline references (Figure 3b,c). This confirms that the short-range coordination environment of four-connected T_d- and four-connected O_h-symmetric Fe^{2+}-nodes is intact in the amorphous network. Specifically, the peak at r = 6.1 Å corresponds to the Fe–Fe distance across bridging im^- or bim^- linker, affirming the presence of a coordination network in ***g*Fe-^{t}Bubipy**. Beyond r = 6.1 Å, however, pair correlations are negligible for ***g*Fe-^{t}Bubipy**, in contrast to the well-defined long-range order in the crystalline reference materials. These findings corroborate the absence of long-range order in ***g*Fe-^{t}Bubipy** and support its characterization as a CRN structure composed of four-connected T_d and O_h nodes.

2.2. Thermal Behavior

TGA of ***g*Fe-^{t}Bubipy** under a N_2 flow demonstrates thermal stability up to 130 °C, with less than 1% weight loss observed below that temperature (Figure S3, Supporting Information). Above 130 °C, mass loss is attributed to the evaporation of organic ligands, which leads to thermal decomposition. Notably, the decomposition temperature of ***g*Fe-^{t}Bubipy** is significantly lower than that of crystalline $Fe_3(im)_6(imH)_2$, where the evaporation of charge-neutral imH ligands begins at ≈225 °C.[17] This difference likely arises from the disordered and defective network structure of ***g*Fe-^{t}Bubipy**, which enhances the thermal mobility and evaporation of organic ligands under the conditions of the TGA experiment.

Differential scanning calorimetry (DSC) measurements were performed under N_2 atmosphere at a scan rate of ±10 °C min^{-1} over the range from 40 to 110 °C to further characterize the

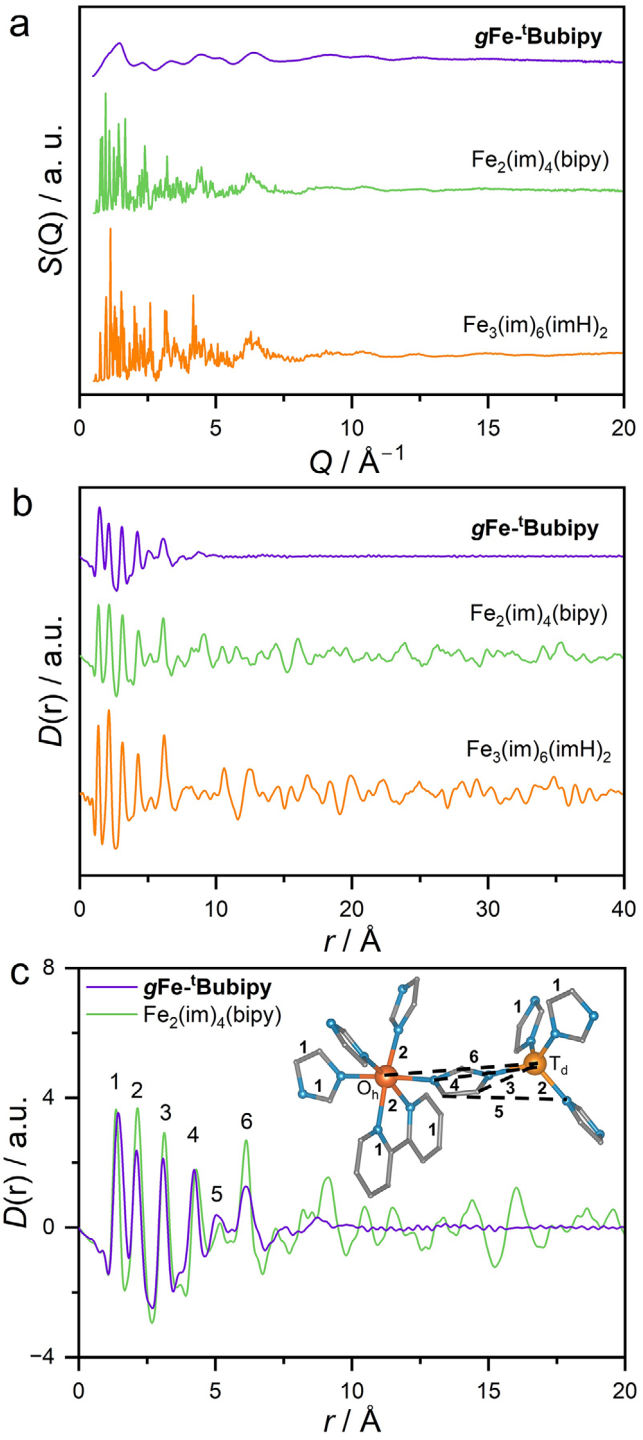

Figure 3. a) X-ray total scattering functions ($S(Q)$) recorded at 30 °C and b) the corresponding PDFs in the form of $D(r)$ of $Fe_3(im)_6(imH)_2$, $Fe_2(im)_4(bipy)$, and ***g*Fe-^{t}Bubipy**. c) Zoom into the low-r region (0–20 Å) of the PDFs of compositionally related materials $Fe_2(im)_4(bipy)$ and ***g*Fe-^{t}Bubipy**. The inset shows the characteristic atom–atom correlations of the crystalline reference compound $Fe_2(im)_4(bipy)$. $Fe^{2+}(O_h)$, $Fe^{2+}(T_d)$, N, and C atoms are shown in dark orange, orange, blue, and gray. H atoms are removed for clarity.

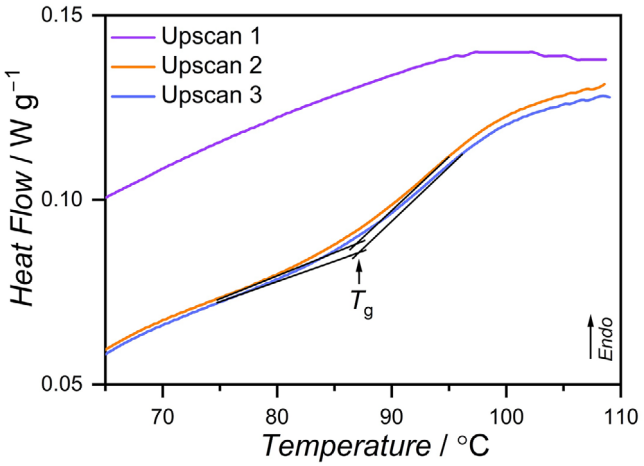

Figure 4. DSC data of ***g*Fe-^{t}Bubipy** showing the glass transition temperature (T_g) ≈85–87 °C.

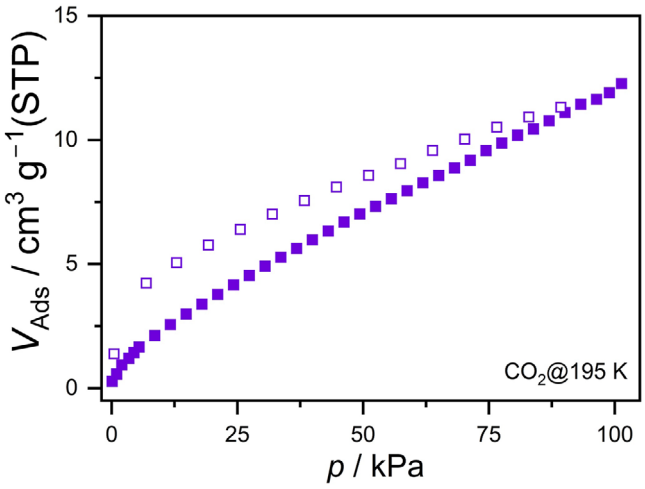

Figure 5. CO_2 sorption isotherms of ***g*Fe-bipy** and ***g*Fe-^{t}Bubipy** collected at 195 K. Filled and empty squares represent the adsorption and desorption branches, respectively.

thermal behavior (**Figure 4**). As expected for amorphous materials, no distinct melting transition is observed during the first heating cycle. Instead, a broad endothermic signal appears, attributed to thermal relaxation within the amorphous network. In the second and third heating cycles, clear glass transition signals are observed, with a glass transition temperature (T_g) of 87 °C. For consistency with previous studies on MOF glasses, T_g was determined as the onset temperature of the calorimetric glass transition signal.[3,15,52] The absence of these features in the first upscan is explained by the need to reset the thermal history of the material during the first heating scan. To confirm the stability of the glassy phases, an additional DSC experiment was conducted, in which ***g*Fe-^{t}Bubipy** was first heated to 90 °C and held at this temperature for 30 min before cooling to ambient temperature. Subsequent heating scans to 105 °C again revealed a clear T_g signal at 85 °C, confirming the stability of the glassy phases and the absence of crystallization during thermal cycling (Figure S4, Supporting Information).

The T_g of ***g*Fe-^{t}Bubipy** is substantially lower than those of typical ZIF glasses, including the only reported Fe^{2+}-based ZIF glass a_gMUV-24 ($Fe(im)_2$), which features a T_g of ≈190 °C. This reduced T_g can be ascribed to the presence of ^{t}Bubipy co-ligands and encapsulated $Fe(Cp)_2$ molecules. The co-ligands may stabilize undercoordinated Fe^{2+} centers and facilitate Fe—N bond dissociation (with N from im^- or bim^-) at lower temperatures, lowering the energy barrier for the glass to transition to the supercooled liquid. This interpretation is in line with recent findings that the addition of H_2O, also acting as a co-ligand, can significantly reduce the T_g of Zn-based ZIF glasses.[53]

2.3. Porosity

Most of the previously reported Zn- and Co-based ZIF glasses feature intrinsic microporosity, making them attractive for gas separation and sensing applications.[1–3,13,19] Typically, the ultramicropores in ZIF glasses are too narrow to allow N_2 adsorption at 77 K. Hence, we examined the microporosity of ***g*Fe-^{t}Bubipy** by CO_2 sorption measurements at 195 K. The total CO_2 uptake (V_{ads}) amounts to 12.3 $cm^3\ g^{-1}$ (STP) at 100 kPa (**Figure 5**). The CO_2 capacity is substantially lower than that of prototypical glasses of the Zn-based ZIF-4 (≈60 $cm^3\ g^{-1}$ (STP)) and ZIF-62 (≈70 $cm^3\ g^{-1}$ (STP)).[2] The shallow increase in CO_2 uptake with increasing pressure suggests predominant adsorption on the external surface of ***g*Fe-^{t}Bubipy** particles. However, the observed hysteresis indicates that some CO_2 molecules may access the ultra-micropores of the CRN structures of the Fe^{2+}-based MOF glass. The reduced porosity of ***g*Fe-^{t}Bubipy** compared to typical ZIF glasses can be attributed to the inclusion of the bulk co-ligand ^{t}Bubipy and encapsulated $Fe(Cp)_2$ molecules, which likely occupy and block the pores of the glass network.

2.4. Magnetic Properties

As the FTIR and PDF data suggest, the random coordination network of ***g*Fe-^{t}Bubipy** features locally ordered Fe^{2+} centers in tetrahedral and octahedral environments interconnected by im^-/bim^- linkers. The rather short Fe—Fe distances of ≈6.1 Å are expected to facilitate the antiferromagnetic exchange between neighboring Fe^{2+} centers through the bridging linkers.[20–25] To investigate the magnetic properties, temperature-dependent field-cooled (FC) and zero-field-cooled (ZFC) magnetization measurements were performed in the temperature range from 300 to 2 K. The ZFC curves were recorded by first cooling the sample down to 2 K in the absence of a field, followed by warming it up at a constant temperature rate (2 K min^{-1}) to 300 K in an applied magnetic field of 0.1 T. The FC curve was subsequently recorded by cooling back to 2 K in the same 0.1 T field.

Magnetic susceptibility (χ_M) data extracted from the ZFC magnetization measurements display Curie-Weiss behavior above 15 K (**Figure 6a**). A least-squares fit of χ_M versus temperature in the range 30–300 K to the Curie-Weiss law ($\chi_M = C/(T-\theta_{CW}) + \chi_0$) yields a Curie constant (C) of 5.491(3) $cm^3\ K\ mol^{-1}$ and a Curie-Weiss temperature (θ_{CW}) of −22.59(3) K (Figure S15 and Table S3, Supporting Information; χ_0 is a temperature-independent term accounting for diamagnetic contributions). The moderately negative θ_{CW} indicates predominant antiferromagnetic interactions

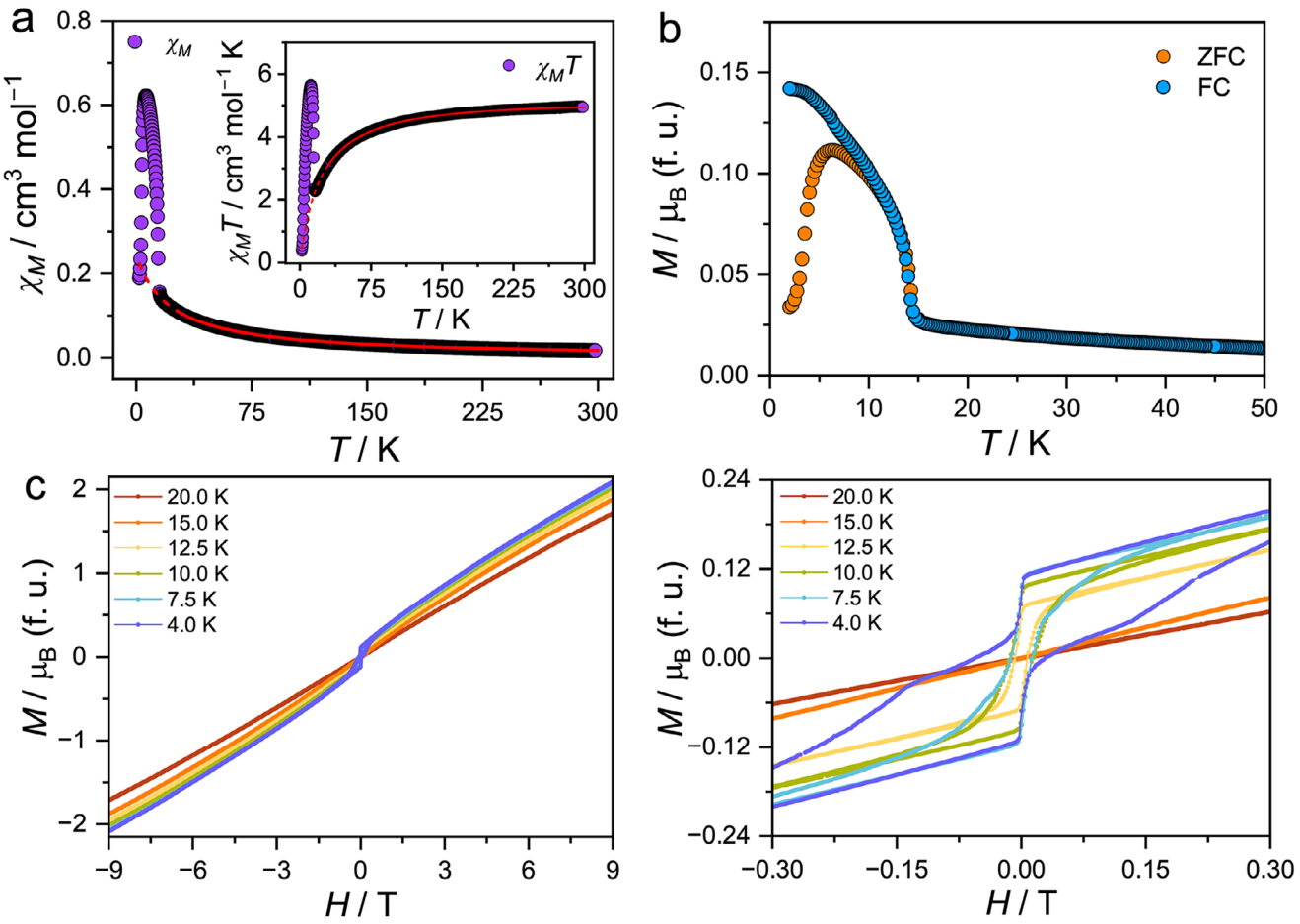

Figure 6. a)Temperature dependence of the molar magnetic susceptibility (χ_M and $\chi_M T$ (inset) obtained from zero field-cooled (ZFC) measurements) of ***g*Fe-^{t}Bubipy** in the range of 2–300 K under a magnetic field of 0.1 T. The red solid lines represent a Curie-Weiss fit to the χ_M versus T data in the range from 30 to 300 K. The red dashed lines are an extrapolation of the fit to lower temperatures. b) Thermal dependence of ZFC and field-cooled (FC) magnetization measurements of ***g*Fe-^{t}Bubipy** in the low temperature range under 0.1 T. c) Isothermal field-dependent magnetization measurements of ***g*Fe-^{t}Bubipy** in the temperature range of 4–20 K. A zoom into the region of the hysteresis loops of the field-dependent magnetization measurements is shown on the right.

between neighboring Fe^{2+} spins. This interpretation is supported by the continuous decrease in the product $\chi_M T$ between 300 and 15 K (Figure 6a, inset).

The extracted Curie constant of ≈5.5 cm^3 K mol^{-1} is smaller than the value expected for two non-interacting HS Fe^{2+} centers per formula unit of $[Fe_2(im)_{3.12}(bim)_{0.88}(^tBubipy)_{0.11}]\cdot[Fe(Cp)_2]_{0.09}$, considering $Fe(Cp)_2$ as diamagnetic due to its LS Fe^{2+}. Assuming two magnetically active HS Fe^{2+} centers per formula unit yields an effective magnetic moment (μ_{eff}) of 4.69 μ_B per Fe^{2+} (calculated via $\mu_{eff} = \sqrt{8\ C/n}$, n = number of HS Fe^{2+} ions per formula unit), below the spin-only theoretical value (μ_{eff} = 4.9 μ_B for S = 2, g = 2.0). However, if the octahedral Fe^{2+} centers coordinated by ^{t}Bubipy adopt an LS configuration, the number of magnetically active Fe^{2+} centers reduces to ≈1.89 per formula unit. This scenario yields μ_{eff} = 4.82 μ_B per Fe^{2+}, much closer to the theoretical spin-only value and comparable with other Fe^{2+}-based materials. This hypothesis is further supported by Mössbauer spectroscopy, which at both 300 and 20 K does not show a doublet characteristic of octahedral HS Fe^{2+}, but may include a minor contribution from octahedral LS Fe^{2+} species (see the Supplementary Information for details).

This magnetic behavior contrasts with the crystalline analog $Fe_2(im)_4(bipy)$, which contains octahedral HS Fe^{2+} centers at room-temperature and undergoes partial spin-crossover between 155 and 130 K.[25] In $Fe_2(im)_4(bipy)$, the LS state of the $[FeN_6]$ units is enthalpically favored, but the rigid lattice imposes structural constraints that stabilize the entropically favored HS state. By contrast, the local structural flexibility and absence of long-range periodicity in the CRN topology of ***g*Fe-^{t}Bubipy** allow for local relaxation into the enthalpically preferred LS state.

Below ≈15 K, the FC and ZFC magnetization measurements show an abrupt increase in magnetization, with pronounced divergence of the FC and ZFC curves below 11.5 K, pointing toward a magnetic transition (Figure 6b). Mössbauer spectra recorded at 15 K and below confirm this transition, exhibiting magnetic hyperfine splitting for tetrahedral HS Fe^{2+} centers due to static or quasi-static local magnetic fields (Figure S16, Supporting Information). Field-dependent isothermal magnetization measurements (±9 T) at temperatures between 4 and 20

K, reveal hysteresis loops below 15 K, with remnant magnetization of 0.12 μ_B per formula unit and coercive fields of 56.2 mT at 4.0 K (Figure 6c). The lack of magnetic saturation even at 9 T indicates significant magnetic frustration, frozen spin disorder, and the presence of energy barriers separating metastable spin configurations.[30,32,34,35,54]

To further elucidate the nature of the magnetic transition, AC susceptibility measurements were conducted in the vicinity of the ZFC magnetization peak, using frequencies (*f*) ranging from 10 Hz to 9984 Hz and an AC magnetic field amplitude of 1 mT (**Figure** 7a,b). The real (χ_M') and imaginary (χ_M'') components of the molar magnetic susceptibility both exhibit frequency dependence, with χ_M' showing an asymmetric peak shape.

The pronounced frequency dependence of χ_M' (in-phase susceptibility) and χ_M'' (out-of-phase susceptibility) indicates spin-glass-like relaxation behavior rather than a sharp transition from a well-ordered antiferromagnetic to a paramagnetic state upon heating.[30,32,34] This behavior can be characterized by a frequency-dependent freezing temperature T_F that reflects the measurement timescale. The frequency dependence is often quantified by looking at the Mydosh parameter given as $\phi = \frac{\Delta T_f}{T_f \times \Delta(\log 2\pi f)}$. Using T_F values defined by the χ_M' peak positions in the range from 10 to 230 Hz, we obtained $\phi \approx 0.0044$. This value lies at the lower end of what Mydosh reported for spin glass systems (0.0045-0.06), and is well below values typical for superparamagnetic nanoparticles ($\phi > 0.1$).[30–32,55] This finding supports the interpretation of the transition as spin-glass freezing driven by interacting, frustrated spins arranged in the CRN topology of ***g*Fe-^{t}Bubipy**.

To analyse the dynamical slowing down in more detail, the frequency dependence of the χ_M'' peak temperatures was fitted using the Vogel–Fulcher law:[56] $\frac{1}{2\pi f} = \tau = \tau_0 \cdot \exp(\frac{E_A}{k_B(T_F - T_0)})$, where τ is the relaxation time (Figure 7c). The fit yielded the thermal activation energy $E_A/k_B = 21(3)$ K and a microscopic attempt time $\tau_0 = 1.1^{2.8}_{0.8}$ ps, both of which are physically reasonable for spin-glass systems. The Vogel–Fulcher temperature $T_0 = 12.75(6)$ K corresponds to the idealized freezing temperature as frequency approaches zero, and its value agrees well with the low-temperature divergence observed in DC magnetization measurements. These results provide strong evidence for cooperative spin freezing and confirm the assignment of the low-temperature magnetic transition in ***g*Fe-^{t}Bubipy** as spin-glass behavior.[56]

The spin-glass behavior in ***g*Fe-^{t}Bubipy** originates from its CRN topology, which inherently includes both even- and odd-membered rings,[57–59] introducing geometric frustration and competing magnetic interactions. Although ≈5.5% of the Fe^{2+} centers adopt a magnetically inactive octahedral LS configuration due to ^{t}Bubipy coordination, the magnetic response is dominated by tetrahedral HS Fe^{2+} centers. Each HS Fe^{2+} center has, on average, 3.78 HS neighbors separated by ≈6.1 Å, promoting superexchange pathways through im^- and bim^- linkers. The encapsulated diamagnetic $Fe(Cp)_2$ molecules contribute negligibly to the overall magnetic behavior. The interplay between structural disorder, predominant HS Fe^{2+} tetrahedral connectivity, and intrinsic topological frustration gives rise to a structurally disordered yet magnetically correlated spin-glass state, setting ***g*Fe-^{t}Bubipy** apart from conventional crystalline MOF magnets.

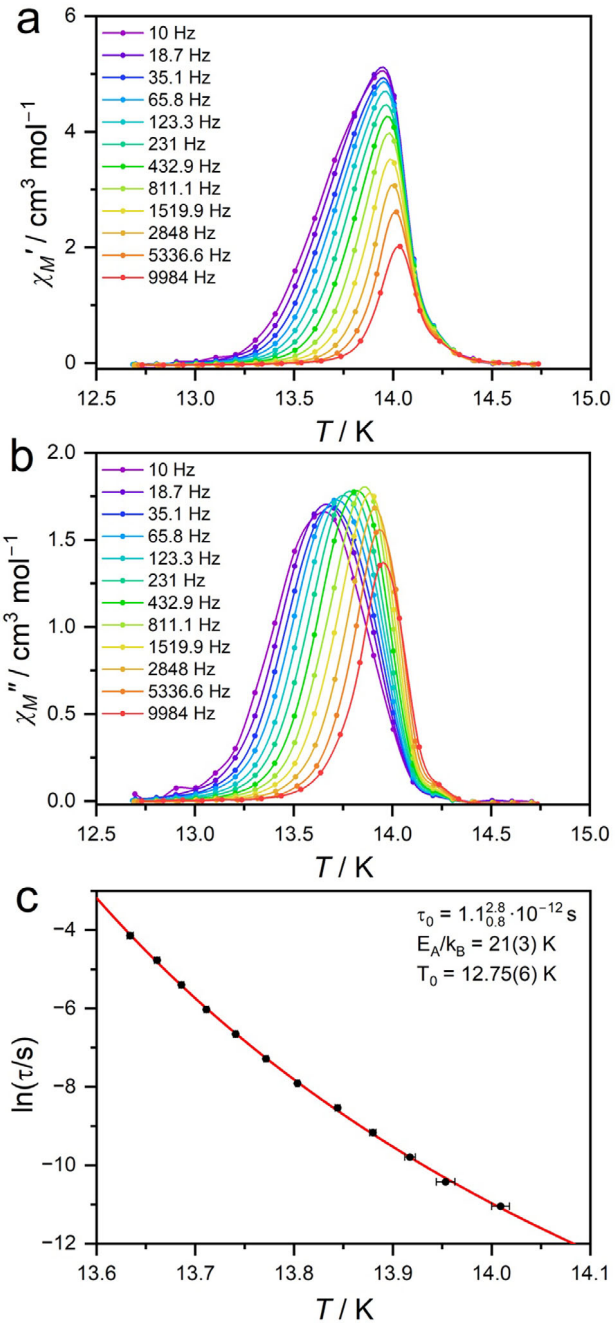

Figure 7. Real a) and imaginary component b) of magnetic AC susceptibility of ***g*Fe-^{t}Bubipy** between 12.7 and 14.7 K recorded at 1 mT. Data have been corrected for frequency-independent background contributions. Lines are a guide to the eye. c) Frequency-dependency of χ_M'' between 10 and 9984 Hz recorded at 1 mT. Data have been interpolated assuming the Vogel–Fulcher law (red line), as explained in the text.

3. Conclusion

In this study, we introduce a solvent-free, one-pot synthesis strategy to prepare an Fe^{2+}-based MOF glass, ***g*Fe-^{t}Bubipy**, with the composition $[Fe_2(im)_{3.12}(bim)_{0.88}(^tBubipy)_{0.11}]\cdot[Fe(Cp)_2]_{0.09}$. This material represents a significant advancement in MOF

glass research, exhibiting a continuous random network topology composed predominantly of four-connected tetrahedral Fe^{2+} nodes, with a minor fraction (≈5.5%) of octahedral Fe^{2+} nodes coordinated by *cis*-coordinating ^{t}Bubipy ligands in a magnetically inactive low-spin state. The octahedral nodes are decorated with *cis*-coordinating ^{t}Bubipy capping ligands and presumably feature a diamagnetic LS configuration. Remarkably, ***g*Fe-^{t}Bubipy** has a very low glass transition temperature (T_g = 87 °C), potentially enabling processing and shaping at moderate temperatures, a key property for future device integration.

The introduced solvent-free method offers significant advantages over earlier melt-quenching methods by enabling the direct synthesis of glassy phases without partial decomposition, thus preventing the formation of unwanted metal and metal oxide nanoparticles, such as Co and CoO, which previously hindered the investigation of the magnetic properties of Co^{2+}-based MOF glasses.[18] Our method for the controlled preparation of Fe^{2+}-based MOF glasses is particularly advantageous for investigating the intrinsic magnetic properties of MOF glasses, a field previously limited by synthetic constraints.

Unlike conventional amorphous magnetic materials, including antiferromagnetic metallic alloys,[60,61] the ***g*Fe-^{t}Bubipy** glass exhibits a notable degree of local structural order, evidenced by PDF analysis. This local order strongly influences its magnetic interactions, resulting in spin-glass behavior with a spin-freezing temperature ≈14 K. Such spin-glass characteristics, emerging directly from the inherent structural disorder and magnetic frustration of the CRN topology, render ***g*Fe-^{t}Bubipy** distinct from existing crystalline and amorphous magnetic solids.

From a fundamental standpoint, ***g*Fe-^{t}Bubipy** provides an exceptional platform for probing the physics of geometric frustration, non-equilibrium dynamics, and cooperative spin freezing in structurally disordered coordination networks. Its CRN topology with four-connected nodes, combined with tunable chemical composition, makes it especially valuable for model studies of spin-glass phenomena, ageing effects, memory and dynamics, and the influence of local structure on macroscopic magnetic responses. Future work will focus on systematically varying the metal-ligand chemistry, altering co-ligand identity, node connectivity, and metal-ion substitution (e.g., Mn^{2+}, Co^{2+}, Ni^{2+}, Cu^{2+}), to tailor the energy landscape and dynamic response of the glassy network. Such studies will deepen our understanding of frustration-driven magnetism in amorphous MOFs and coordination networks and may guide the rational design of next-generation MOF-based magnetic materials with tailored and unconventional spin dynamics.

Supporting Information

Supporting Information is available from the Wiley Online Library or from the author.

Acknowledgements

The Deutsche Forschungsgemeinschaft, DFG, (projects 434514047 and 447344931) and the DFG priority program 1928 COORNETs are acknowledged for funding. Further financial support by the DFG via the CRC/TRR 247 (Project-ID 388390466, sub-project B02) and the CRC/TRR 270 (Project-ID 405553726, sub-project B05) is gratefully acknowledged. JBW and PK acknowledge the Fonds der Chemischen Industrie for Kekulè Fellowships. WLX acknowledges the China Scholarship Council for a PhD scholarship (CSC No. 202008110208). The authors acknowledge DESY (Hamburg, Germany), a member of the Helmholtz Association HGF, for the provision of experimental facilities. X-ray total scattering of this research was carried out at PETRA III (DESY) on beamline P02.1 (proposal I-20220350) and at beamline I15-1 of Diamond Light Source (DLS), Oxon., UK (Proposal CY31642). The authors thank the beamline scientists Dr. Alexander Schoekel (PETRA III / P02.1) and Dr. Phil Chater (DLS / I15-1) for their support with the X-ray total scattering experiments. The authors gratefully acknowledge the computing time provided on the Linux HPC cluster at Technical University Dortmund (LiDO3), partially funded in the course of the Large-Scale Equipment Initiative by the DFG as project 271512359.

Conflict of Interest

The authors declare no conflict of interest.

Author Contributions

C.D. and S.H. designed the project. C.D. carried out all material syntheses and characterization, including PXRD, FTIR, ^{1}H NMR spectroscopy, TGA, DSC, and CO_2 gas sorption. S.S. and J.L. performed the magnetic measurements and Mössbauer spectroscopy. J.B.W. conducted DFT calculations and analyzed the FTIR data. X-ray total scattering measurements at DESY and Diamond Light Source were performed by C.D., W.L.X., P.K., and R.P. The initial draft of the manuscript was prepared by C.D. and S.H. All authors contributed to the revision of the manuscript and approved the final version.

Data Availability Statement

The data that support the findings of this study are available in the supplementary material of this article.

Keywords

amorphous materials, glasses, magnetism, metal–organic frameworks, spin freezing

Received: July 11, 2025
Published online:

[1] L. Frentzel-Beyme, M. Kloß, P. Kolodzeiski, R. Pallach, S. Henke, *J. Am. Chem. Soc.* **2019**, *141*, 12362.
[2] L. Frentzel-Beyme, P. Kolodzeiski, J. B. Weiß, A. Schneemann, S. Henke, *Nat. Commun.* **2022**, *13*, 7750.
[3] W. L. Xue, P. Kolodzeiski, H. Aucharova, S. Vasa, A. Koutsianos, R. Pallach, J. Song, L. Frentzel-Beyme, R. Linser, S. Henke, *Nat. Commun.* **2024**, *15*, 4420.
[4] C. Das, S. Henke, *Nat. Mater.* **2023**, *22*, 809.
[5] N. Ma, S. Kosasang, A. Yoshida, S. Horike, *Chem. Sci.* **2021**, *12*, 5818.
[6] N. Ma, S. Impeng, S. Bureekaew, N. Morozumi, M.-a. Haga, S. Horike, *J. Am. Chem. Soc.* **2023**, *145*, 9808.
[7] Y. Wang, H. Jin, Q. Ma, K. Mo, H. Mao, A. Feldhoff, X. Cao, Y. Li, F. Pan, Z. Jiang, *Angew. Chem., Int. Ed.* **2020**, *59*, 4365.

[8] Z. Yang, Y. Belmabkhout, L. N. McHugh, D. Ao, Y. Sun, S. Li, Z. Qiao, T. D. Bennett, M. D. Guiver, C. Zhong, *Nat. Mater.* **2023**, *22*, 888.
[9] O. Smirnova, S. Hwang, R. Sajzew, L. Ge, A. Reupert, V. Nozari, S. Savani, C. Chmelik, M. R. Reithofer, L. Wondraczek, J. Kärger, A. Knebel, *Nat. Mater.* **2024**, *23*, 262.
[10] S. Li, R. Limbach, L. Longley, A. A. Shirzadi, J. C. Walmsley, D. N. Johnstone, P. A. Midgley, L. Wondraczek, T. D. Bennett, *J. Am. Chem. Soc.* **2019**, *141*, 1027.
[11] T. To, S. S. Sørensen, M. Stepniewska, A. Qiao, L. R. Jensen, M. Bauchy, Y. Yue, M. M. Smedskjaer, *Nat. Commun.* **2020**, *11*, 2593.
[12] A. Qiao, H. Tao, M. P. Carson, S. W. Aldrich, L. M. Thirion, T. D. Bennett, J. C. Mauro, Y. Yue, *Opt. Lett.* **2019**, *44*, 1623.
[13] O. Smirnova, R. Sajzew, S. J. Finkelmeyer, T. Asadov, S. Chattopadhyay, T. Wieduwilt, A. Reupert, M. Presselt, A. Knebel, L. Wondraczek, *Nat. Commun.* **2024**, *15*, 5079.
[14] J. Li, J. Wang, Q. Li, M. Zhang, J. Li, C. Sun, S. Yuan, X. Feng, B. Wang, *Angew. Chem., Int. Ed.* **2021**, *60*, 21304.
[15] T. D. Bennett, Y. Yue, P. Li, A. Qiao, H. Tao, N. G. Greaves, T. Richards, G. I. Lampronti, S. A. T. Redfern, F. Blanc, O. K. Farha, J. T. Hupp, A. K. Cheetham, D. A. Keen, *J. Am. Chem. Soc.* **2016**, *138*, 3484.
[16] R. Gaillac, P. Pullumbi, K. A. Beyer, K. W. Chapman, D. A. Keen, T. D. Bennett, F. X. Coudert, *Nat. Mater.* **2017**, *16*, 1149.
[17] L. León-Alcaide, R. S. Christensen, D. A. Keen, J. L. Jordá, I. Brotons-Alcázar, A. Forment-Aliaga, G. Mínguez Espallargas, *J. Am. Chem. Soc.* **2023**, *145*, 11258.
[18] L. Frentzel-Beyme, M. Kloß, R. Pallach, S. Salamon, H. Moldenhauer, J. Landers, H. Wende, J. Debus, S. Henke, *J. Mater. Chem. A* **2019**, *7*, 985.
[19] W. L. Xue, C. Das, J. B. Weiß, S. Henke, *Angew. Chem., Int. Ed.* **2024**, *63*, 202405307.
[20] S. J. Rettig, A. Storr, D. A. Summers, R. C. Thompson, J. Trotter, *J. Am. Chem. Soc.* **1997**, *119*, 8675.
[21] S. J. Rettig, A. Storr, D. A. Summers, R. C. Thompson, J. Trotter, *Can. J. Chem.* **1999**, *77*, 425.
[22] S. J. Rettig, V. Sánchez, A. Storr, R. C. Thompson, J. Trotter, *Inorg. Chem.* **1999**, *38*, 5920.
[23] S. J. Rettig, V. Sánchez, A. Storr, R. C. Thompson, J. Trotter, *J. Chem. Soc., Dalton Trans.* **2000**, https://doi.org/10.1039/B002574G.
[24] W. M. Reiff, V. Sanchez, R. C. Thompson, A. Storr, *Polyhedron* **2001**, *20*, 1243.
[25] B. O. Patrick, W. M. Reiff, V. Sánchez, A. Storr, R. C. Thompson, *Inorg. Chem.* **2004**, *43*, 2330.
[26] T. Storr, J. R. Thompson, B. O. Patrick, W. M. Reiff, A. Storr, R. C. Thompson, *Polyhedron* **2016**, *108*, 80.
[27] J. López-Cabrelles, S. Mañas-Valero, I. J. Vitórica-Yrezábal, P. J. Bereciartua, J. A. Rodríguez-Velamazán, J. C. Waerenborgh, B. J. C. Vieira, D. Davidovikj, P. G. Steeneken, H. S. J. van der Zant, G. Mínguez Espallargas, E. Coronado, *Nat. Chem.* **2018**, *10*, 1001.
[28] J. López-Cabrelles, S. Mañas-Valero, I. J. Vitórica-Yrezábal, M. Šiškins, M. Lee, P. G. Steeneken, H. S. J. van der Zant, G. Mínguez Espallargas, E. Coronado, *J. Am. Chem. Soc.* **2021**, *143*, 18502.
[29] C. A. M. Mulder, A. J. van Duyneveldt, J. A. Mydosh, *Phys. Rev. B* **1981**, *23*, 1384.
[30] K. Binder, A. P. Young, *Rev. Mod. Phys.* **1986**, *58*, 801.
[31] D. Chowdhury, *Spin Glasses and Other Frustrated Systems*, World Scientific, London **1986**, https://doi.org/10.1142/0223.
[32] J. A. Mydosh, *Spin Glasses: An Experimental Introduction*, Taylor & Francis, London **1993**, https://doi.org/10.1201/9781482295191.
[33] C. J. O'Connor, *Research Frontiers in Magnetochemistry*, World Scientific, London **1993**, https://doi.org/10.1142/1894.
[34] A. P. Ramirez, *Annu. Rev. Mater. Res.* **1994**, *24*, 453.
[35] M. J. P. Gingras, C. V. Stager, N. P. Raju, B. D. Gaulin, J. E. Greedan, *Phys. Rev. Lett.* **1997**, *78*, 947.
[36] D. Walton, A. McCleary, C. V. Stager, N. P. Raju, *Phys. Rev. B* **1999**, *59*, 135.
[37] R. Clérac, S. O'Kane, J. Cowen, X. Ouyang, R. Heintz, H. Zhao, M. J. Bazile, K. R. Dunbar, *Chem. Mater.* **2003**, *15*, 1840.
[38] D. Sherrington, S. Kirkpatrick, *Phys. Rev. Lett.* **1975**, *35*, 1792.
[39] Z. Yin, Y. Zhao, S. Wan, J. Yang, Z. Shi, S. X. Peng, M. Z. Chen, T. Y. Xie, T. W. Zeng, O. Yamamuro, M. Nirei, H. Akiba, Y. B. Zhang, H. B. Yu, M. H. Zeng, *J. Am. Chem. Soc.* **2022**, *144*, 13021.
[40] M. Z. Chen, J. Li, S. Liao, Y. H. Guo, T. Liu, R. F. Ma, T. Y. Xie, W. D. Liu, S. X. Peng, X. Kuang, Z. Yin, Y. Zhao, M. H. Zeng, *Angew. Chem., Int. Ed.* **2023**, *62*, 202305942.
[41] J. S. Gardner, B. D. Gaulin, S. H. Lee, C. Broholm, N. P. Raju, J. E. Greedan, *Phys. Rev. Lett.* **1999**, *83*, 211.
[42] W. E. Buschmann, J. S. Miller, *Inorg. Chem.* **2000**, *39*, 2411.
[43] M. F. Thorne, M. L. R. Gómez, A. M. Bumstead, S. Li, T. D. Bennett, *Green Chem.* **2020**, *22*, 2505.
[44] J. López-Cabrelles, J. Romero, G. Abellán, M. Giménez-Marqués, M. Palomino, S. Valencia, F. Rey, G. Mínguez Espallargas, *J. Am. Chem. Soc.* **2019**, *141*, 7173.
[45] E. M. Kober, B. P. Sullivan, T. J. Meyer, *Inorg. Chem.* **1984**, *23*, 2098.
[46] J. Ferguson, F. Herren, E. R. Krausz, M. Maeder, J. Vrbancich, *Coord. Chem. Rev.* **1985**, *64*, 21.
[47] S. Cerfontaine, L. Troian-Gautier, Q. Duez, J. Cornil, P. Gerbaux, B. Elias, *Inorg. Chem.* **2021**, *60*, 366.
[48] L. M. Zheng, X. Fang, K. H. Lii, H. H. Song, X. Q. Xin, H. K. Fun, K. Chinnakali, I. Abdul Razak, *J. Chem. Soc., Dalton Trans.* **1999**, https://doi.org/10.1039/A809738K.
[49] T. P. Gerasimova, S. A. Katsyuba, *Dalton Trans.* **2013**, *42*, 1787.
[50] M. U. Munshi, J. Martens, G. Berden, J. Oomens, *J. Phys. Chem. A* **2020**, *124*, 2449.
[51] M. U. Munshi, G. Berden, J. Oomens, *J. Phys. Chem. A* **2025**, *129*, 1318.
[52] J. Hou, M. L. Ríos Gómez, A. Krajnc, A. McCaul, S. Li, A. M. Bumstead, A. F. Sapnik, Z. Deng, R. Lin, P. A. Chater, D. S. Keeble, D. A. Keen, D. Appadoo, B. Chan, V. Chen, G. Mali, T. D. Bennett, *J. Am. Chem. Soc.* **2020**, *142*, 3880.
[53] S. S. Sørensen, A. K. R. Christensen, E. A. Bouros-Bandrabur, E. S. Andersen, H. F. Christiansen, S. Lang, F. Cao, M. F. U. Jalaludeen, J. F. S. Christensen, W. M. W. Winters, B. P. Andersen, A. B. Nielsen, N. C. Nielsen, D. B. Ravnsbæk, P. K. Kristensen, Y. Yue, M. M. Smedskjaer, *Chem. Mater.* **2024**, *36*, 2756.
[54] J. E. Greedan, *J. Mater. Chem.* **2001**, *11*, 37.
[55] Y. Y. Zhang, M. H. Zeng, Y. Qi, S. Y. Sang, Z. M. Liu, *Inorg. Chem. Commun.* **2007**, *10*, 33.
[56] S. Kundu, A. Pal, A. Chauhan, K. Patro, K. Anand, S. Rana, V. G. Sathe, A. G. Joshi, P. Pal, K. Sethupathi, B. R. K. Nanda, P. Khuntia, *Phys. Rev. Mater.* **2022**, *6*, 104401.
[57] R. Gaillac, P. Pullumbi, T. D. Bennett, F. X. Coudert, *Chem. Mater.* **2020**, *32*, 8004.
[58] N. Castel, D. André, C. Edwards, J. D. Evans, F. X. Coudert, *Digit. Discov.* **2024**, *3*, 355.
[59] T. C. Nicholas, D. F. Thomas du Toit, L. A. M. Rosset, D. M. Proserpio, A. L. Goodwin, V. L. Deringer, *arXiv preprint* **2025**, https://doi.org/10.48550/arXiv.2503.24367.
[60] J. M. D. Coey, *J. Appl. Phys.* **1978**, *49*, 1646.
[61] R. Hasegawa, *J. Magn. Magn. Mater.* **1991**, *100*, 1.